Effect of NaCl-Na_2CO_3 Inorganic Salt Ratio on the Performance of Water-Soluble Composite Salt Cores

Miao Wang1, 2, Fu-chu Liu1, 2*

1. School of Mechanical Engineering and Electronic Information, China University of Geosciences, Wuhan 430074, China;
2. Shenzhen Research Institute, China University of Geosciences, Guangdong Shenzhen 518057, China
*Corresponding address: e-mail: liufuchu@cug.edu.cn

Abstract: An experimental investigation was conducted on the inorganic salt ratio of NaCl-Na_2CO_3 water-soluble composite salt cores for low-melting-point aluminum (magnesium) alloy die-casting components. Water-soluble composite salt cores were fabricated using micro-extrusion 3D printing technology. The effects of different salt ratios on the performance of the composite salt cores were systematically analyzed based on evaluation metrics including surface morphology, X/Y/Z-direction shrinkage rates, flexural strength, porosity, water-soluble rate, and moisture absorption rate. Results indicate that when the NaCl content is 80 mol% and Na_2CO_3 is 20 mol%, the sintered salt core exhibits a complete structure, stable morphology, flexural strength of 21.91 MPa, porosity of 8.99%, water-soluble rate of 2.03 g/(s·m²) in 80 ℃ water, and a 24 h moisture absorption rate of 10.9%, demonstrating excellent comprehensive performance. This optimized ratio meets the diverse performance requirements of soluble core materials for practical engineering applications and shows promising prospects for industrial use.

Keywords: low-melting-point aluminum (magnesium) alloys; water-soluble composite salt cores; inorganic salt ratio; micro-extrusion 3D printing; surface morphology; flexural strength; water-soluble rate

1 Introduction

Aluminum (magnesium) alloys have been widely utilized in aerospace, automotive manufacturing, and electronic industries due to their low density, high specific strength, and excellent corrosion resistance [1-3]. In recent years, driven by the growing demand for lightweight design, aluminum (magnesium) alloy die castings have played an increasingly critical role in the fabrication of high-performance structural components. Particularly in the automotive sector, the application of aluminum (magnesium) alloy die castings significantly contributes to vehicle weight reduction, thereby enhancing fuel efficiency and driving range [4-6]. However, with the rising demand for complex thin-walled castings, traditional metal cores have encountered numerous challenges in the production of hollow aluminum (magnesium) alloy castings, including difficulties in core removal and limitations in achieving intricate geometries [7-9]. Meanwhile, collapsible sand cores, constrained by inadequate strength and difficulties associated with post-casting removal, fail to meet the comprehensive requirements for mechanical strength, dimensional precision, and removability demanded by high-performance castings [10-12]. Therefore, the development of advanced core materials that offer a combination of high strength, excellent solubility, and good formability is of significant engineering importance and practical value for the manufacture of hollow aluminum (magnesium) alloy die castings.

Compared to traditional sand cores, water-soluble salt cores fabricated using inorganic salts as the matrix material offer distinct advantages, including moderate melting points, favorable mechanical properties, ease of dissolution in water, and low production costs. These cores can withstand the elevated temperatures and pressures encountered during the die-casting process and can be rapidly removed after casting through simple water dissolution, thereby significantly enhancing both the production efficiency and final quality of complex hollow aluminum (magnesium) alloy die castings [13-15].

Due to variations in physicochemical properties among different inorganic salt systems, their performance differs markedly in terms of sintering densification, mechanical strength, solubility, and moisture resistance. Consequently, for

specific application requirements, the development of water-soluble salt core systems with tunable properties, stable formability, and outstanding integrated performance is critical for improving the manufacturing quality of complex aluminum (magnesium) alloy die castings, expanding the application scope of die-casting technology, and driving the advancement of high-end equipment manufacturing. Compared to single-component salt cores, composite salt cores—through the rational combination of different inorganic salts—allow for more precise tailoring of melting behavior, sintering characteristics, microstructural evolution, and mechanical properties [16-18]。

Research on water-soluble salt core systems has explored various inorganic salt combinations. TU et al. [18] employed a molten gravity casting process to comparatively analyze the performance characteristics of KCl salt cores, KNO_3 salt cores, and binary composite water-soluble salt cores composed of 20 mol% KCl and 80 mol% KNO_3. The results indicated that, compared to single-component salt cores, the binary composite cores exhibited superior overall performance, with minimal surface cracks and wrinkles, a flexural strength of up to 21.2 MPa, and moisture absorption as low as 0.568% in 24 hours. Xiao et al. [19] utilized extrusion-based 3D printing technology to fabricate high-strength composite water-soluble salt cores consisting of 30 mol% Na_2SO_4 and 70 mol% NaCl by incorporating alumina powder as a reinforcing agent, enabling the production of hollow composite aluminum alloy castings. Wang et al. [20] calculated the interfacial energies of various inorganic salts based on first-principles calculations and validated the findings through molten casting experiments. Their results demonstrated that the interfacial bonding between NaCl and Na_2SO_4 was more stable, and the binary salt cores exhibited the highest flexural strength when the molar ratio of NaCl to Na_2SO_4 was 7:3.

Although considerable progress has been made in developing water-soluble salt core materials based on different inorganic salt systems, there remains a critical need to design salt core systems with enhanced formability, improved mechanical strength, excellent dissolution performance, and superior moisture resistance to meet the application requirements for low-melting-point aluminum (magnesium) alloy die castings. In addition, conventional fabrication methods for water-soluble salt cores, such as molten casting [21], compaction-sintering [22], and conventional binder-based molding [23], are often limited by low forming precision, high incidence of internal defects, and insufficient adaptability for complex structural components [19, 24], which restricts the widespread application of water-soluble salt cores in the manufacturing of complex hollow castings. Therefore, the development of novel forming technologies to improve both the precision and performance of water-soluble salt cores has become an urgent issue.

In response to these challenges, this paper systematically investigates the influence of inorganic salt ratios on the properties of NaCl-Na_2CO_3 composite salt cores using micro-extrusion 3D printing technology. Surface morphology, shrinkage rates along the X/Y/Z directions, flexural strength, porosity, water-soluble rate, and moisture absorption rate are employed as the primary evaluation metrics to comprehensively assess the performance of composite salt cores under different salt ratio conditions. The aim is to elucidate the synergistic mechanisms by which inorganic salt ratios regulate the microstructural evolution and macroscopic properties of water-soluble composite salt cores, optimize their mechanical strength and dissolution behavior, and ultimately achieve simultaneous improvements in formability and service performance. The research results provide theoretical foundations and technical support for the design and fabrication of high-performance soluble cores for complex hollow die castings of low-melting-point aluminum (magnesium) alloys, further advancing the research depth and application scope of water-soluble salt core materials, and offering significant academic and engineering value.

2 Experimental materials and methods

2.1 Materials

NaCl powder (D_{50} = 10.17 μm, Fengzhihu Salt Research Laboratory Technology (Jiangsu)., Ltd., China) and Na_2CO_3 powder (D_{50} = 6.49 μm, Fengzhihu Salt Research Laboratory Technology (Jiangsu)., Ltd., China) were used as the base materials. The physicochemical properties of the inorganic salts are summarized in Tab. 1, and their powder morphologies and particle size distributions are shown in Fig. 1.

A polyvinylpyrrolidone (PVP-k60, Shandong Yousuo Chemical Technology Co., Ltd., China) solution was used as the binder, while ammonium polyacrylate (Shanghai YuanYe Biotechnology Co., Ltd., China) served as the dispersant. Anhydrous ethanol was employed as the carrier liquid, and an organosilicon-based defoamer (Wuhan Zhuo Yan Technology Co., Ltd., China) was added to eliminate bubbles generated during the slurry preparation process.

Tab. 1 Physicochemical Properties of Inorganic Salt Materials

Inorganic salt	Content (%)	Density (g/cm³)	melting point (℃)	particle size (μm)
NaCl	≥ 97.5	2.17	801	10.169
Na_2CO_3	≥ 98.0	2.54	858	6.487

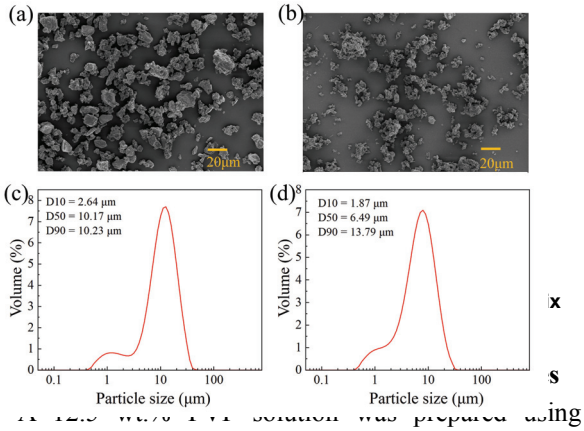

anhydrous ethanol as the solvent. A specified mass of NaCl and Na_2CO_3 powders was added to the PVP solution and stirred until fully wetted. Subsequently, ammonium polyacrylate and an organosilicon-based defoamer were introduced dropwise, followed by thorough stirring to obtain a premixed slurry.

The premixed slurry was then transferred into a ball milling jar and processed using a planetary ball mill (QM-QX, Nanjing Labstar Technology Industrial Co., Ltd., China) at a rotation speed of 300 r/min for 12 hours. After milling, a homogeneous composite salt-based slurry suitable for micro-extrusion 3D printing was obtained. The compositions of the salt-based slurries with different inorganic salt ratios are listed in Tab. 2.

The well-mixed slurry was loaded into the extrusion barrel of a laboratory-developed micro-extrusion 3D printing system. The movement trajectory of the printing nozzle and the extrusion conditions were controlled via slicing software installed on the system's host computer. Following the predefined path, the salt-based slurry was deposited layer by layer onto the substrate to form green bodies of water-soluble composite salt cores, with dimensions of 60 mm × 10 mm × 6 mm.

After 12 hours of natural drying, the green bodies were transferred to a constant-temperature drying oven (DZF-6020, Shanghai Jinghong Experimental Equipment Co., Ltd., China) and dried at 80□ °C for 12 hours. Subsequently, a stepwise sintering process was conducted in a high-temperature furnace (YMG1600–40, Shanghai Yanmai Technology Co., Ltd., China) as follows: heating at a rate of 1□ °C/min to 360□ °C and holding for 1 hour to thoroughly remove anhydrous ethanol and decompose additives; followed by heating at 3□ °C/min to 600□ °C with a 1-hour dwell time; further heating at 5□ °C/min to 640□ °C with a 0.5-hour hold; and finally furnace cooling to room temperature. The process flowchart is shown in Fig. 2.

2.3 Characterization

The top surface of the sintered salt core samples was observed using a super depth-of-field microscope (RX-100, Hirox Co., Ltd., Japan). The dimensions of the samples before and after sintering were measured using a vernier caliper. The sintering shrinkage rate of the salt core was calculated using the Equation (1):

$$L = \frac{l_1 - l_2}{l_1} \times 100\% \quad (1)$$

Where, L is the sintering shrinkage of the salt core (%), l_1 is the size of the billet (mm), l_2 is the size of the sintered body (mm).

The flexural strength of the water-soluble salt core samples was determined based on the maximum load at fracture, measured using a microcomputer-controlled electronic universal testing machine (ETM105D-T, Shenzhen Wance Test Equipment Co., Ltd., China). The three-point bending method was employed with a support span of 30 mm and a loading rate of 0.05 mm/min. The flexural strength was calculated according to Equation (2).

$$\sigma = \frac{3PL}{2bh^2} \quad (2)$$

Where, σ is the flexural strength of the salt core specimen (MPa), P is the maximum load on the specimen at fracture (N), L is the span between the two support points (mm), b is the width of the specimen (mm), h is the height of the specimen (mm).

The porosity of the salt core samples was determined using the Archimedes drainage method. A density balance (JA5003, Shanghai Sunny Hengping Scientific Instrument Co., Ltd., China) was employed to measure the mass of the dry sample in air, the mass of the kerosene-saturated sample in air, and the mass of the kerosene-saturated sample immersed in kerosene. The porosity was calculated according to Equation (3).

$$P_a = \frac{m_2 - m_1}{m_2 - m_3} \times 100\% \quad (3)$$

Where, P_a is the porosity of the salt core specimen (%),

m_1 is the dry weight of the salt core specimen in air (g), m_2 is the mass of the specimen in air saturated with kerosene (g), m_3 is the mass of the specimen in kerosene saturated with kerosene (g).

Tab. 2 Formulation of Salt-Based Slurries at Various Inorganic Salt Ratios

Group	Inorganic salt ratio	NaCl (wt.%)	Na_2CO_3 (wt.%)	12.5% PVP solution (wt.%)	Ammonium polyacrylate (wt.%)	Silicone defoamer (g)
1	10mol%NaCl -90 mol%Na_2CO_3	3.81	62.19			
2	20mol%NaCl -80 mol%Na_2CO_3	8	58			
3	30mol%NaCl -70 mol%Na_2CO_3	12.61	53.39			
4	40mol%NaCl -60 mol%Na_2CO_3	17.74	48.26			
5	50mol%NaCl -50 mol%Na_2CO_3	23.46	42.54	33.5	0.5	0.1
6	60mol%NaCl -40 mol%Na_2CO_3	29.88	36.12			
7	70mol%NaCl -30 mol%Na_2CO_3	37.16	28.84			
9	80mol%NaCl -20 mol%Na_2CO_3	45.41	20.59			
9	90mol%NaCl -10 mol%Na_2CO_3	54.94	11.06			

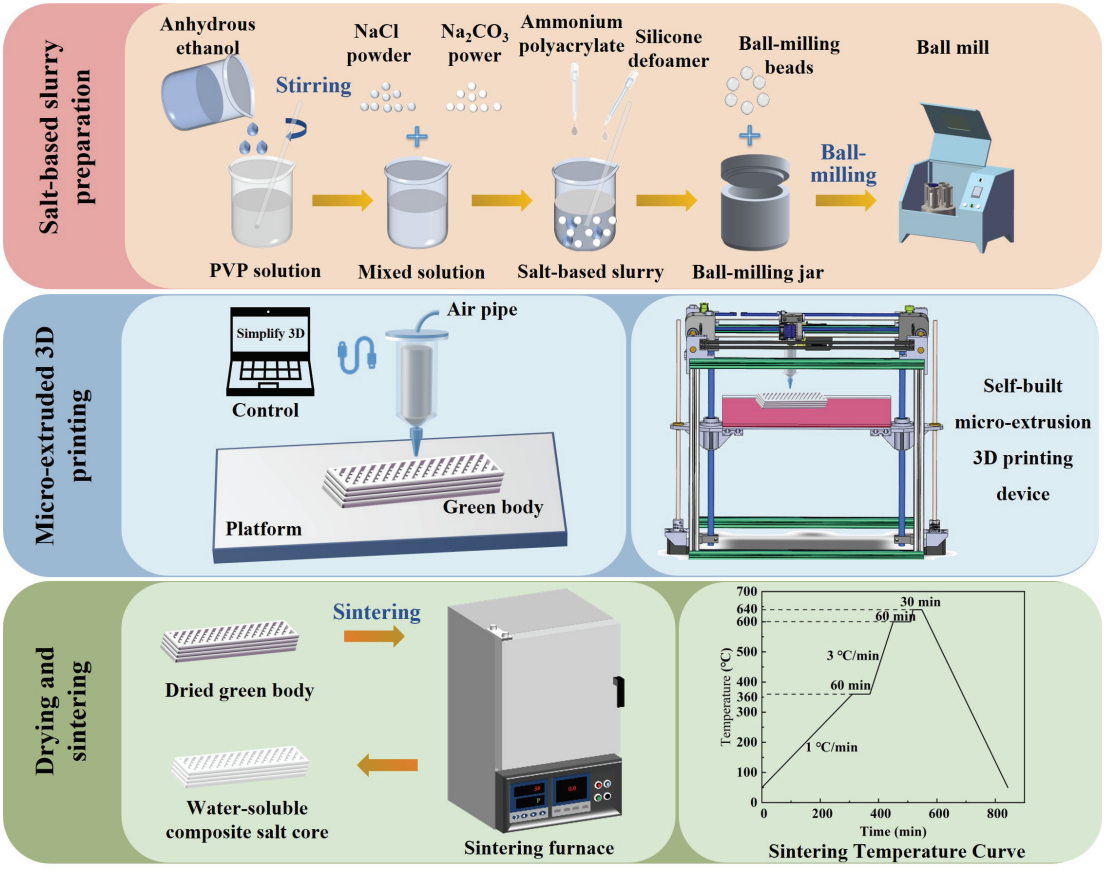

Fig. 2: Process Flow Diagram for Micro-Extrusion 3D Printing of Water-Soluble Composite Salt Cores

The water-soluble rate of the salt core samples was tested using a digital constant-temperature water bath (HH-1, Shanghai Lichen Bangxi Instrument Technology Co., Ltd., China) under static water conditions at 80□ °C. The water-soluble rate at 80□ °C was calculated according to Equation (4). Additionally, the salt core samples were placed in a desiccator with controlled relative humidity maintained at 85%-90%. The 24-hour moisture absorption rate was determined according to Equation (5).

$$k = \frac{m}{s \times t} \tag{4}$$

Where, k is the Water-soluble rate of the salt core specimen (g/(min·m^2)), m is the salt core specimen mass (g), s is the salt core specimen surface area (mm^2), t is the salt core specimen completely dissolved in 80 ℃ constant temperature static water (s).

$$\varphi = \frac{G_1 - G_0}{G_0} \tag{5}$$

Where, φ is the moisture absorption rate of the salt core specimen (%), G_0 is the initial mass of the salt core specimen (g), G_1 is the mass of the salt core after being placed in the hygroscopic bottle for 24h (g).

3 Results and discussion

3.1 Surface morphology

To facilitate comparison of the bending behavior of water-soluble composite salt cores with different inorganic salt ratios after sintering, the side surface morphologies of the cores were recorded, as shown in Figure 3. Due to the occurrence of melting deformation during sintering at 640□ °C, the upper surface morphologies of the composite salt cores with 50 mol% NaCl-50 mol% Na_2CO_3 and 60 mol% NaCl-40 mol% Na_2CO_3 compositions are presented in Fig. 3(e) and Fig. 3(f), respectively.

As shown in Fig. 3, when the NaCl content in the NaCl-Na_2CO_3 binary composite salt cores ranged from 30 mol% to 60 mol%, varying degrees of melting, deformation, and even fracture were observed after sintering, with the 50 mol% NaCl-50 mol% Na_2CO_3 composite cores exhibiting the most severe melting and deformation.

In contrast, when the NaCl content was within the ranges of 10 mol%-20 mol% or 70 mol%-90 mol%, only slight deformation occurred, with the 20 mol% NaCl-80 mol% Na_2CO_3 and 80 mol% NaCl-20 mol% Na_2CO_3 composite cores showing the least deformation and best morphology retention.

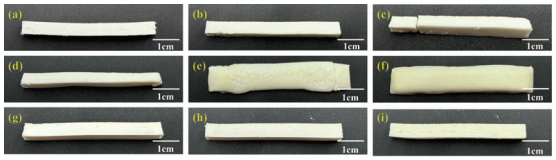

Fig. 3: Side and Top Surface Morphologies of Sintered NaCl-Na_2CO_3 Composite Salt Cores with Different NaCl Contents: (a) 10 mol%; (b) 20 mol%; (c) 30 mol%; (d) 40 mol%; (e) 50 mol%; (f) 60 mol%; (g) 70 mol%; (h) 80 mol%; (i) 90 mol%

The differences in deformation behavior are primarily attributed to the phase diagram characteristics of the NaCl-Na_2CO_3 binary system and the interactions between the two components. As shown in the phase diagram of the salt core system (Fig. 4), a eutectic reaction occurs between NaCl and Na_2CO_3, with a eutectic temperature of approximately 635□ °C. When the composition approaches the eutectic point (approximately 50 mol% NaCl-50 mol% Na_2CO_3), the system can undergo melting at relatively low temperatures, leading to significant flow, collapse, and even fracture of the composite salt cores during the sintering process. In contrast, when the NaCl content is relatively low (10 mol%-20 mol%) or high (70 mol%-90 mol%), the composition deviates from the eutectic point, thereby restricting melting behavior and enhancing structural stability, which significantly reduces the degree of deformation after sintering. Moreover, the amount and distribution of the molten phase at different compositions also affect the mechanical support capability of the salt cores, further influencing their macroscopic deformation behavior.

The surface morphologies of composite salt cores with different NaCl-Na_2CO_3 ratios were examined using a three-dimensional super-depth digital microscope, and the results are presented in Fig. 5. As observed from the surface morphology images, when the NaCl content is within the range of 50 mol%-60 mol%, the composite salt cores exhibit an overall non-uniform surface structure, characterized not only by extensive melting and collapse but also by the presence of localized granular or raised features, resembling crystallization phenomena. This behavior may be attributed to the localized recrystallization and aggregation of NaCl or Na_2CO_3 crystals upon cooling of the molten phase during the sintering process. Due to the substantial amount of molten phase generated near the eutectic composition, enhanced solute migration during sintering likely leads to local supersaturation within the liquid phase, thereby

promoting heterogeneous nucleation and crystal deposition. Such microscopic crystallization further disrupts the surface integrity of the salt cores and exacerbates non-uniform deformation at the macroscopic scale. In contrast, when the NaCl content falls within 10 mol%-20 mol% or 70 mol%-90 mol%, the composite salt cores exhibit relatively smooth and uniform surfaces, with only a few minor pores or slight undulations observed, indicating better morphological stability and structural integrity during the sintering process at these compositions.

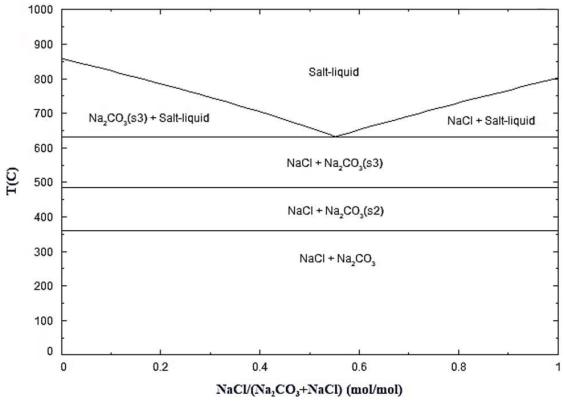

Fig. 4: Phase Diagram of the NaCl-Na_2CO_3 Binary System

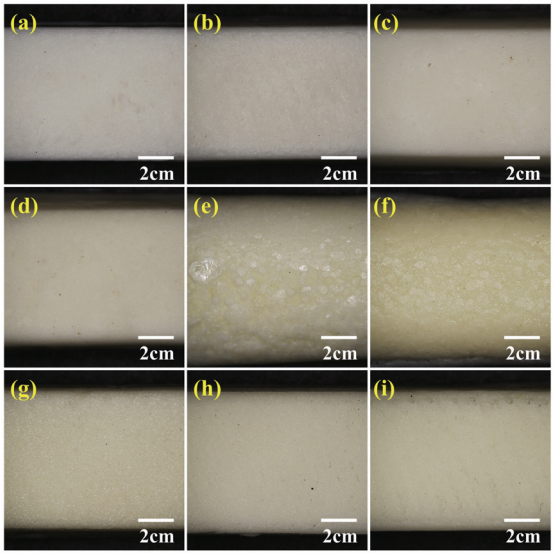

Fig. 5: Surface Morphologies of Sintered NaCl-Na_2CO_3 Composite Salt Cores with Different NaCl Contents Captured by 3D Microscopy: (a) 10 mol%; (b) 20 mol%; (c) 30 mol%; (d) 40 mol%; (e) 50 mol%; (f) 60 mol%; (g) 70 mol%; (h) 80 mol%; (i) 90 mol%.

3.2 Mechanical Performance

The shrinkage rates of the composite salt cores along the X, Y, and Z directions after sintering with different NaCl-Na_2CO_3 ratios are shown in Fig. 6. It can be observed that in the X and Y directions, the shrinkage rates exhibit a trend of being lower at intermediate NaCl contents and higher at both lower and higher ends. When the NaCl content increases from 10 mol% to 40 mol%, the shrinkage rates in the X and Y directions gradually decrease, while the shrinkage rate in the Z direction progressively increases. This behavior indicates that, within this composition range, the degree of melting becomes more pronounced with increasing NaCl content, resulting in a reduction in height (Z-axis) while the dimensions in the X and Y directions expand. Conversely, as the NaCl content increases from 60 mol% to 90 mol%, the shrinkage rates in the X and Y directions gradually increase, whereas the shrinkage rate in the Z direction decreases, suggesting a diminished degree of melting with higher NaCl content in this range. Moreover, due to severe collapse and even fracture in some specimens, dimensional measurements after sintering could not be reliably obtained, leading to abnormal fluctuations in the shrinkage data for samples with intermediate NaCl contents.

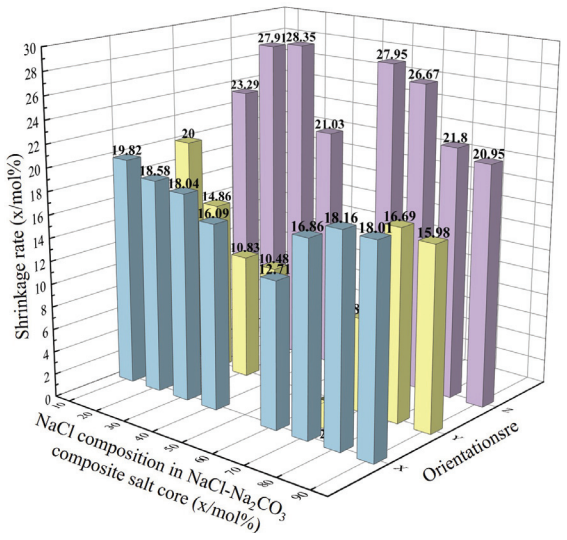

Fig. 6: Sintering Shrinkage Rates in X, Y, and Z Directions of NaCl-Na_2CO_3 Composite Salt Cores with Different NaCl Contents

The flexural strength of the composite salt cores after sintering with different NaCl-Na_2CO_3 ratios is presented in Fig. 7. The results show that when the NaCl content is within the range of 10 mol% to 40 mol%, the flexural strength remains relatively low and varies only slightly, ranging from 10.30 MPa to 13.16 MPa. Among these compositions, the 20 mol% NaCl-80 mol% Na_2CO_3 group exhibits a slightly higher flexural strength compared to the others. As the NaCl content increases from 60 mol% to 90 mol%, the flexural strength first increases and then decreases, with the strength rising

from 11.24 MPa to a peak of 21.91 MPa, followed by a decline to 16.18 MPa. Notably, the composite salt core with 80 mol% NaCl-20 mol% Na_2CO_3 exhibits the highest flexural strength among all tested compositions.

Fig. 8 shows the variations in porosity of the composite salt cores with different NaCl-Na_2CO_3 ratios. As illustrated, the trend in porosity changes closely mirrors that of the flexural strength. When the NaCl content is in the range of 10 mol% to 40 mol%, the porosity remains relatively low with minimal variation, with the 20 mol% NaCl-80 mol% Na_2CO_3 group exhibiting a slightly higher porosity of 5.71%. As the NaCl content increases from 60 mol% to 90 mol%, the porosity first increases and then decreases, specifically rising from 4.37% to a maximum of 8.99%, followed by a decrease to 5.21%. Among the tested compositions, the 80 mol% NaCl-20 mol% Na_2CO_3 composite salt core exhibits the highest porosity, indicating that the water-soluble salt cores with this ratio formed a more significant pore structure during the sintering process.

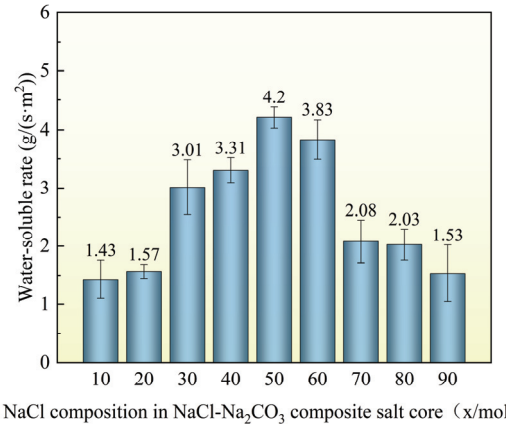

Fig. 7: Flexural Strength of NaCl-Na_2CO_3 Composite Salt Cores with Different NaCl Contents

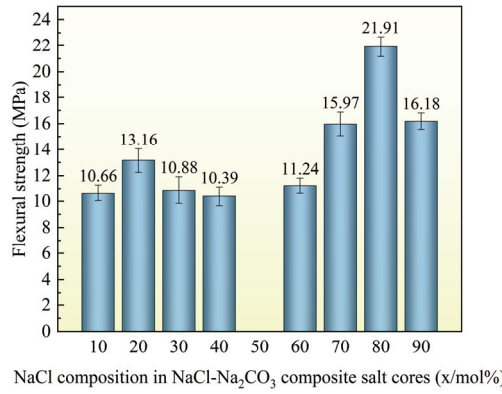

Fig. 8: Porosity of NaCl-Na_2CO_3 Composite Salt Cores with Different NaCl Contents

3.3 Moisture absorption and water solubility rate

Fig. 9 presents the variations in the water-soluble rate at 80□ °C for the composite salt cores with different NaCl-Na_2CO_3 ratios. The results indicate that the water-soluble rate initially increases and then decreases with increasing NaCl content. Among the tested compositions, the 50 mol% NaCl-50 mol% Na_2CO_3 composite salt core exhibits the highest water-soluble rate, reaching 4.20 g/(s·m²), suggesting the most favorable dissolution behavior under these conditions. In contrast, the 10 mol% NaCl-90 mol% Na_2CO_3 composite salt core shows the lowest water-soluble rate, only 1.43 g/(s·m²), indicating a slower dissolution process, which may be attributed to its denser structure or the reduced solubility associated with lower NaCl content.

The variation in the water-soluble rate is primarily influenced by the ratio of NaCl to Na_2CO_3 in the composite salt core and the microstructure formed after sintering. As NaCl is a highly soluble salt, its content plays a dominant role in the overall dissolution behavior. When the NaCl content is low (e.g., 10 mol%-40 mol%), the composite salt core is predominantly composed of Na_2CO_3. Since the water-soluble rate of Na_2CO_3 is significantly lower than that of NaCl, and the sintered samples at this composition exhibit a relatively dense structure with low porosity, this limits the diffusion path of water, resulting in a lower water-soluble rate. At a NaCl content of 50 mol%, the composite salt core undergoes melting and collapse during sintering, which leads to the formation of a complex pore network inside the core. This facilitates water infiltration and accelerates NaCl dissolution, thereby achieving the peak water-soluble rate. When the NaCl content is further increased to 60 mol%-90 mol%, the degree of melting in the composite salt core decreases. During this phase, the high NaCl content leads to grain coarsening or a looser structure, which consequently results in a decrease in the water-soluble rate.

The variation in the moisture absorption rate of the composite salt cores with different inorganic salt ratios is shown in Fig. 10. Overall, as the NaCl content increases from 10 mol% to 90 mol%, the moisture absorption rate of the composite salt cores exhibits minimal variation, fluctuating between 9.69% and 11.3%. This indicates that the composite salt cores exhibit a relatively stable response to environmental humidity.

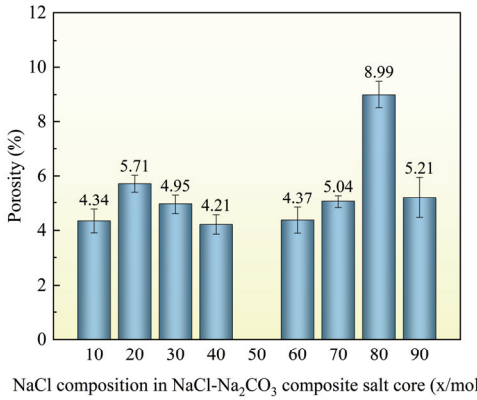

Fig. 9: Water Solubility Rate of NaCl-Na_2CO_3 Composite Salt Cores with Different NaCl Contents

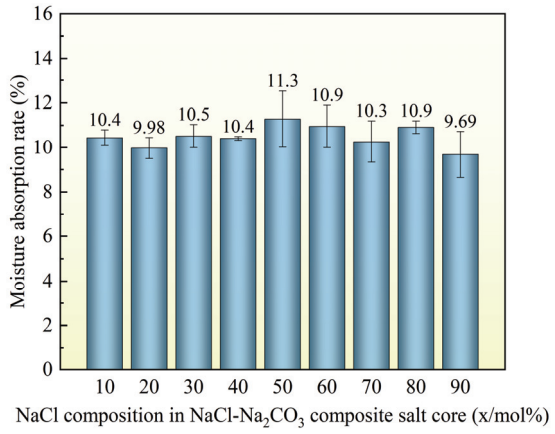

Fig. 10: Hygroscopicity of NaCl-Na_2CO_3 Composite Salt Cores with Different NaCl Contents

4 Conclusions

(1) The sintering morphology of the composite salt cores is significantly influenced by the NaCl content. When the NaCl content is in the range of 30 mol% to 60 mol%, which is near the eutectic composition, melting and collapse are more likely to occur during sintering, leading to poor structural integrity and even fracture. The surface exhibits uneven melting and crystal precipitation. In contrast, when the NaCl content is in the range of 10 mol% to 20 mol% and 70 mol% to 90 mol%, the system is far from the eutectic composition, restricting the melting behavior. The morphology is well-maintained, with a relatively smooth surface and only a small number of micropores or slight undulations.

(2) The shrinkage behavior and flexural strength of the composite salt cores exhibit certain regularities with changes in NaCl content. The shrinkage rate in the X and Y directions is lower in the middle compositions (30 mol% to 60 mol%) and higher at both ends (10 mol% to 20 mol% and 70 mol% to 90 mol%). The Z-direction shrinkage follows the opposite trend. Flexural strength with the increase of NaCl content showed a basic stability first, then rise and then decline of the law of change, 80 mol% NaCl-20 mol% Na_2CO_3 group has the highest flexural strength of 21.91 MPa, the porosity is also up to the maximum (8.99%), suggesting that the moderate pore structure contributes to the mechanical properties of the enhancement.

(3) The moisture absorption rate of the composite salt cores changes little with NaCl content, remaining stable between 9.69% and 11.3%, indicating good adaptability to environmental humidity. The water-soluble rate, however, increases initially and then decreases with the increase in NaCl content. The 50 mol% NaCl-50 mol% Na_2CO_3 sample exhibits the highest water-soluble rate, reaching 4.20 g/(s·m²), as a result of significant melting during sintering and the formation of a complex pore structure, which enhances its dissolution performance. However, when the NaCl content is in the range of 30 mol% to 60 mol%, the sintered salt cores have poor structural integrity, prone to collapse or fracture, severely affecting their shaping quality and application reliability, making them unsuitable for practical engineering applications.

(4) Considering the structural morphology, mechanical properties, and dissolution behavior comprehensively, the composite salt core with an 80 mol% NaCl-20 mol% Na_2CO_3 ratio exhibits intact structure and stable morphology after sintering. It has a flexural strength of 21.91 MPa, a porosity of 8.99%, a Water-soluble rate of 2.03 g/(s·m²) in static water at 80°C, and a 24-hour moisture absorption rate of 10.9%. This composition shows excellent performance in terms of morphological stability, flexural strength, and water-soluble rate, demonstrating promising overall properties with high potential for engineering applications.

Acknowledgments

The authors would like to thank the support of Guangdong Basic and Applied Basic Research Foundation (No.2024A1515013258), the National Nature Science Foundation of China (No. 52375395), Shenzhen Fundamental Research Program of China (No. JCYJ20220818102601004),
the Fundamental Research Funds for National Universities, China University of Geosciences (Wuhan) (No.2024XLB25 and No.2024XLB26), the Teaching Laboratory Open Fund Project of China University of Geosciences (Wuhan) (No. SKJ2023125 and No. SKJ2024121), the National Undergraduate Innovation and Entrepreneurship Training Program (No.

202410491047, No. 202410491048, No. 202410491058, No. S202410491017, No. S202410491102, No. X202410491055)

Conflicts of interest

The authors declare that they have no known competing financial interests or personal relationships that could have appeared to influence the work reported in this paper.

References

[1] Zhang J Y, Pan J C, Zhang W, et al. Application and analysis of new TIG remelting welding process on magnesium-aluminum alloy equipment [J]. Metallurgy and Materials, 2025, 45(03): 7-9.

[2] Xing Z, Lin H, Fan S, et al. Study on the microstructure evolution and deformation strengthening mechanism of aluminum -magnesium alloys under continuous deformation [J]. Journal of Materials Research and Technology, 2025, 35: 2283-97.

[3] Malakhov A, Saikov I, Denisov I, et al. Study of microstructure evolution in the aluminum-magnesium alloy AlMg6 after explosive welding and heat treatment [J]. The International Journal of Advanced Manufacturing Technology, 2024, 134(9): 4451-63.

[4] Jing Q H, Chen J, Peng L M, et al. Research progress in joining of carbon fiber-reinforced polymer composites and aluminum/ magnesium alloys [J]. Journal of Materials Engineering, 2022, 50(01): 15-24.

[5] Zhang L J, Liu C C, Yang J L. A kind of lightweight magnesium alloy wheel hub liquid die forging forming process and molds [J]. Forging & Metalforming, 2023, (17): 47-9.

[6] Mokhtari M A, Nikzad M H. Multi-objective optimization and comparison of machine learning algorithms for the prediction of tensile properties of aluminum-magnesium alloy [J]. Materials Today Communications, 2024, 40: 109476.

[7] Vesenjak M, Duarte I, Baumeister J, et al. Bending performance evaluation of aluminium alloy tubes filled with different cellular metal cores [J]. Composite Structures, 2020, 234: 111748.

[8] Chen L, Feng L, Wang Y P, et al. A Guide Mechanism of Core-pulling Rapid Replacement for Die Casting Die [J]. Special Casting & Nonferrous Alloys, 2021, 41(06): 784-6.

[9] Wang Y, Ding P. Design of Die Casting Die for the Metal Faucet Valve Body [J]. Special Casting & Nonferrous Alloys, 2018, 38(09): 965-7.

[10] Liu J J, Lou Y C, Yin S K, et al. Application of Modified Ester Cured Sodium Silicate Sand to High Manganese Steel Casting [J]. Foundry, 2020, 69(12): 1331-4.

[11] Song L, Zhang H K, Wang C G, et al. Research on Modified and Compound Hardened Water Glass Binder [J]. Foundry, 2018, 67(10): 871-4.

[12] Anwar N, Sappinen T, Jalava K, et al. Comparative experimental study of sand and binder for flowability and casting mold quality [J]. Advanced Powder Technology, 2021, 32(6): 1902-10.

[13] Aslan İ, Can A. Investigation of the Mechanical Properties of Water-Soluble Salt Cores Produced by Binder Jetting Additive Manufacturing [J]. International Journal of Metalcasting, 2025.

[14] Zhang J, Li Y, Song L, et al. Effect of Mold Temperature and Pouring Temperature on the Crack Behavior of Composite Water-Soluble Salt Cores [J]. International Journal of Metalcasting, 2024, 18(4): 3221-30.

[15] Liu X Y, Liu W H, Wang X T, et al. Composition Optimization and Strengthening Mechanism of High-Strength Composite Water-Soluble Salt Core for Foundry [J]. International Journal of Metalcasting, 2022, 16(4): 1809-16.

[16] Li Y, Song L, Liu W, et al. Study on the Effects and Mechanism of Multi-particle Size Hybrid Alumina Particles on the Strength, Water Solubility, and Cracking Tendency of NaCl–Na2CO3 Binary Salt Cores [J]. International Journal of Metalcasting, 2025.

[17] Yaokawa J, Miura D, Anzai K, et al. Strength of Salt Core Composed of Alkali Carbonate and Alkali Chloride Mixtures Made by Casting Technique [J]. MATERIALS TRANSACTIONS, 2007, 48(5): 1034-41.

[18] Tu S, Fan Z T, Liu F C, et al. Preparation and properties of a binary composite water-soluble salt core for zinc alloy by die casting [J]. Chinese Journal of Engineering, 2017, 39(11): 1692-8.

[19] Xiao X, Gong X, Zhao J, et al. Preparation of Alumina Powder-Reinforced High-Strength Salt Cores Produced via 3D Direct Printing for Aluminum Alloy Casting [J]. International Journal of Metalcasting, 2024, 18(3): 2210-24.

[20] Wang X T, Liu W H, Liu X Y, et al. First-Principles Calculation and Mechanical Properties of NaCl–Na2SO4 Composite Water-Soluble Salt Core [J]. International Journal of Metalcasting, 2023, 17(1): 263-71.

[21] Yu J, You Z Y, Jiang A X, et al. Microstructure and Properties of Soluble Salt Core Prepared by Molten Casting [J]. Special Casting & Nonferrous Alloys, 2023, 43(07): 898-902.

[22] Jiang W, Dong J, LOU L, et al. Preparation and Properties of a Novel Water Soluble Core Material [J]. Journal of Materials Science & Technology, 2010, 26(3): 270-5.

[23] Xiao Z, Harper L T, Kennedy A R, et al. A water-soluble core material for manufacturing hollow composite sections [J]. Composite Structures, 2017, 182: 380-90.

[24] Chen Z, Fan S, Peng L, et al. Fabrication and Characterization of High-strength Water-soluble Composite Salt Cores via Layered Extrusion Forming [J]. International Journal of Metalcasting, 2023, 17(2): 988-97.